

---

# Architecture-Agnostic Masked Image Modeling – From ViT back to CNN

---

Siyuan Li<sup>1\*</sup> Di Wu<sup>1\*</sup> Fang Wu<sup>2</sup> Zelin Zang<sup>1</sup> Kai Wang<sup>3</sup>  
Lei Shang<sup>3</sup> Baigui Sun<sup>3</sup> Hao Li<sup>3</sup> Stan.Z.Li<sup>1</sup>  
<sup>1</sup>AI Lab, Westlake University <sup>2</sup>Columbia University  
<sup>3</sup>DAMO Academy, Alibaba Group

## Abstract

Masked image modeling (MIM), an emerging self-supervised pre-training method, has shown impressive success across numerous downstream vision tasks with Vision transformers (ViT). Its underlying idea is simple: a portion of the input image is randomly masked out and then reconstructed via the pre-text task. However, why MIM works well is not well explained, and previous studies insist that MIM primarily works for the Transformer family but is incompatible with CNNs. In this paper, we first study interactions among patches to understand what knowledge is learned and how it is acquired via the MIM task. We observe that MIM essentially teaches the model to learn better middle-level interactions among patches and extract more generalized features. Based on this fact, we propose an Architecture-Agnostic Masked Image Modeling framework (A<sup>2</sup>MIM), which is compatible with not only Transformers but also CNNs in a unified way. Extensive experiments on popular benchmarks show that our A<sup>2</sup>MIM learns better representations and endows the backbone model with the stronger capability to transfer to various downstream tasks for both Transformers and CNNs.

## 1 Introduction

Supervised deep learning with large-scale annotated data has witnessed an explosion of success in computer vision (CV) [28, 25] and natural language processing (NLP) [42]. However, large amount of high-quality annotations are not always available in real-world applications. Learning representations without supervision by leveraging pre-text tasks has become increasingly popular.

In CV, early self-supervised learning approaches [57, 14, 19] aim to capture invariant features through predicting transformations applied to the same image. However, these methods rely on vision ad-hoc heuristics, and representations thus learned are less generic for downstream tasks. Recently, the contrastive learning-based approaches to self-supervised learning have witnessed significant progress, even outperforming supervised methods on several downstream tasks. Despite different contrasting mechanisms, contrastive-based methods learn generic representation by minimizing the distance between two augmented views of the same image in the embedded space.

More recently, inspired by the masked autoencoding in NLP such as GPT [37] and BERT [13], Masked Image Modeling (MIM) methods [22, 45, 52] have brought about new advances for self-supervised pre-training for CV tasks. The transition from human language understanding to NLP masked autoencoding is quite natural because the filling of missing words in a sentence requires relatively comprehensive semantic understanding. In analogy, humans can understand and imagine masked content by visually filling the missing structures in an image containing occluded parts. The underlying idea of MIM is thus to randomly mask out a proportion of the image and then recover the masked patches.

---

\*First two authors have equal contribution

Different from contrastive learning, which yields a clustering effect from pre-training by pulling similar samples and pushing away dissimilar samples, MIM pre-training methods have not been extensively explored in the context of the expected knowledge learned or how this knowledge is acquired. Moreover, the success of existing MIM methods is largely confined to Vision Transformer (ViT) structures [16]. Current MIM frameworks are not generic in terms of network architectures because it is not straightforward to directly apply mask token [13] and positional embedding to convolutional neural networks (CNNs).

In this work, we carry out systematic experiments and show that MIM as pre-training task essentially teaches the model to better learn middle-level interactions between patches for more generalized feature extraction regardless of the underlying network structure. Compared to the local texture features learned by low-level interactions between patches, more complex features such as shape and edge could be extracted via middle-level interactions among patches. The interaction of patches could be considered as information fusion via both convolution operation of a CNN and the self-attention mechanism of a Transformer. That is to say, CNN and Transformer should both benefit from better middle-level interactions with MIM as the pre-text task.

To bridge the gap of MIM in terms of network architectures based on our extensive experimental analysis, we propose an Architecture-Agnostic Masked Image Modeling framework (A<sup>2</sup>MIM) that focuses on enhancing the middle-level interaction capabilities of the network. Specifically, we mask the input image with the mean RGB value and place the mask token at intermediate feature maps of the network. In addition, we propose a loss in the Fourier domain to further enhance the middle-level interaction capability of the network. Our contributions are summarized as follows:

- We conducted systematic experiments and showed the essence of MIM is to better learn middle-level interactions between patches but not reconstruction quality.
- We proposed a novel MIM-based framework dubbed A<sup>2</sup>MIM that bridges the gap between CNNs and Transformers. To the best of our knowledge, we are the first to carry out MIM on CNNs that outperforms contrastive learning counterparts.
- Extensive experiments with both Transformers and CNNs on ImageNet-1K and public benchmarks for various downstream tasks show that our method achieves significant performance improvement on pre-trained representation quality than state-of-the-arts.

## 2 Related Work

Learning representations without supervision by leveraging pre-text tasks has become increasingly popular. This section briefly discusses two types of popular self-supervised vision pre-training approaches: contrastive learning and autoregressive modeling.

### 2.1 Contrastive Learning

Contrastive learning learns instance-level discriminative representations by extracting invariant features over distorted views of the same data. MoCo [23] adopted a large momentum memory bank to introduce enough negative samples, while SimCLR [8] replaced the vanilla memory bank [48] by a larger batch size. BYOL [21] and its variants [9, 10] further eliminates the requirement of negative samples, using various techniques to avoid representation collapse. Besides pairwise contrasting, SwAV [5] clusters the data while enforcing consistency between multi-augmented views of the same image. Barlow Twins [55] proposed to measure the cross-correlation matrix of distorted views of the same image to avoid representation collapsing. Meanwhile, some effects have been made on top of contrastive methods to improve pre-training quality for specific downstream tasks [51, 50, 38, 47]. With the recent emergence of Transformers as an alternative to CNN for CV tasks, MoCo.V3 [10] and DINO [6] adopted ViT [16] in self-supervised pre-training to replace of CNN backbones.

### 2.2 Autoregressive Modeling

Autoencoders are a typical type of neural network architecture that allows representation learning with no annotation requirement [26]. A standard autoencoder contains an encoder that maps the input to a representation and a decoder that outputs a reconstructed version of the input using the learned representation. By forcing denoising property onto the learned representations, denoising

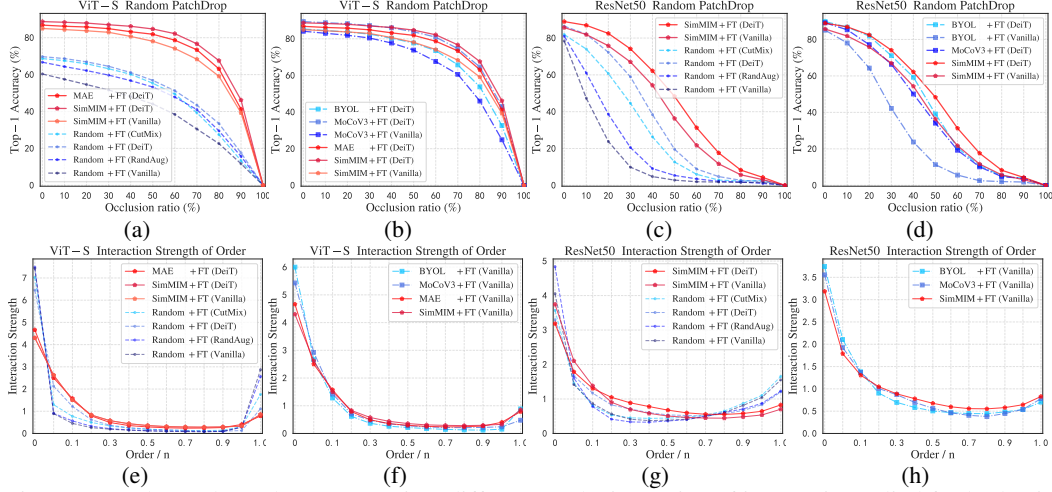


Figure 1: (a)(b)(c)(d): Robustness against different occlusion ratios of images is studied for both ViT-S and ResNet-50 under different experimental settings (see Section 3.1). (e)(f)(g)(h): Distributions of the interaction strength  $J^{(m)}$  is explored for both ViT-S and ResNet-50 under different experimental settings. The label indicates the pre-training method + fine-tuning augmentation used, random stands for random weight initialization. Appendix B provides more results.

autoencoders [43, 44] are a family of autoencoders that reconstruct the uncorrected input signal with a corrupted version of the signal as input. In addition to directly reconstructing the corrupted image, CIM [18] also proposed to predict whether each visual token is replaced by a generator sample or not. Generalizing the notion of denoising autoregressive modeling, masked predictions attracted the attention of both the NLP and vision community. BERT [13] performs masked language modeling where the task is to predict the randomly masked input tokens. Representations learned by BERT as pre-training generalize well to various downstream tasks. For CV, inpainting tasks [36] to predict large missing regions using convolutional networks is proposed to learn representation without supervision. Inpainting the original color of images with removed color channels is also proposed to learn generic representations [57]. With the introduction of the Vision Transformer (ViT), iGPT [7] predicts succeeding pixels given a sequence of pixels as input. MAE [22] and BEiT [4] mask out random patches of the input image and reconstruct the missing patches with ViT. Compared to MAE, MaskFeat [45] and simMIM [52] adopt linear layers as the prediction head instead of another Transformer as in MAE. MaskFeat proposed to use HOG as the prediction target instead of RGB value as used in MAE. Some methods [17, 60, 2] combine the idea of contrastive learning with MIM. SplitMask [17] proposed to use half of the image pixels to predict the other half while applying InfoNCE loss [41] across the corresponding latent representations. MSN [2] matches the representation of an image view containing randomly masked patches to the representation of the original unmasked image. Similarly, iBOT [60] adopts the Siamese framework to combine self-distillation with MIM. Moreover, data2vec [3] proposed a framework that applies the masked prediction idea for either speech, NLP, or CV. In this work, we focus on MIM itself, and thus, the combination of MIM with contrastive learning is beyond the scope of this paper.

### 3 Intriguing Properties of Masked Image Modeling

#### 3.1 Does MIM Bring Occlusion Robustness?

The higher degree of freedom of the receptive field of vision Transformers induced by the self-attention mechanism is believed to be the reason for Transformers outperforming CNNs. Compared to CNN, Transformers gain tremendous performance improvement with carefully designed image augmentation techniques such as RandAug[11], and CutMix[54]. Random erasing[58] randomly removes part of the image and replace with Gaussian noise while Cutmix randomly removes part of the image and replaces the corresponding region with a patch from another image. Similarly, as in most MIM pre-training tasks, some patches of images are masked out and replaced with a learnable mask token. *We hypothesize that MIM as pre-training task as well as similar data augmentations enhance the network’s robustness towards occlusion and thus enables the network with a more*

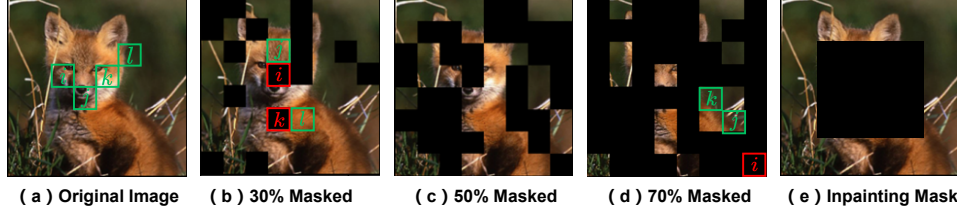


Figure 2: (a) Four patches ( $i, j, k, l$ ) interact with each other and forms a contour or edge pattern of the fox for image categorization. (b) Image with 30% masking ratio. Masked patches  $i$  and  $k$  interact with neighboring patches  $j$  and  $l$  to predict the missing patches. (c) Image with 50% masking ratio. Masked patches are forced to interact with middle-level interactions for the MIM task. (d) Image with 70% masking ratio. Masked Patch  $i$  interacts with longer-range patches  $j$  and  $k$  forming an edge pattern. (e) A typical masking pattern for existing inpainting tasks.

*generalized feature extraction ability.* To verify our hypothesis, we design an occlusion robustness test. Let  $x \in \mathbb{R}^{3 \times H \times W}$  be an input image and  $y \in \mathbb{R}^C$  be its corresponding label, where  $C$  is the class number. Consider a classification task  $y = f(x)$  where  $f$  denotes a neural network, the network is considered robust if the network outputs the correct label given an occluded version of the image  $x'$ , namely  $y = f(x')$ . For occlusion, we consider the patch based random masking as adopted in most MIM works [22, 52, 45]. In particular, we split the image of size  $224 \times 224$  into patch size  $16 \times 16$  and randomly mask  $M$  patches out of the total number of  $N$  patches. The occlusion ratio could then be defined as  $\frac{M}{N}$ . We conduct experiments on ImageNet-100 (IN-100) [29] with both Transformer and CNN with different settings. Without loss of generality, we choose ViT-S [16] and ResNet-50[25] as the network architecture. We compare robustness under the following settings: (a) random weight initialization with no image augmentation applied, (b) random weight initialization with different image augmentations applied, (c) MIM pre-training as weight initialization with and without image augmentations applied and (d) Contrastive learning pre-training as weight initialization with and without image augmentations applied. We report the average top-1 accuracy across five runs trained with different settings under various occlusion ratios in Figure 1. The results reported in Figure 1(a) show significantly robust performance of MIM as pre-training against random weight initialization for ViT-S. MIM pre-trained models are robust and give comparable accuracy up to 80% occlusion ratio as compared to a drastic accuracy drop of models with random weight initialization. It can be also seen that by applying augmentations as used in DeiT[40] further improves the model robustness. For random weight initialization, we notice that all patch-removing alike augmentations boost the robustness as the accuracy curve shows a convex trend with augmentations. A similar phenomenon could be observed for CNN (ResNet-50) in Figure 1(c). Compared with the concave shape of model with random weight initialization, MIM pre-trained CNN models demonstrate a convex curve indicating a huge robustness gain. It can be found in Figure 1(d) that compared to contrastive learning, MIM shows a more convex trend of accuracy curve, which indicates a better occlusion robustness capability.

### 3.2 Middle-level Interactions for Generalized Feature Extraction

In the previous subsection, we showed that the MIM task improves occlusion robustness for both Transformers and CNNs. However, it remains unclear to us that how occlusion robustness relates to knowledge learned via MIM. Note that existing MIM works adopt a medium or high masking ratio [52, 22] (e.g., 60% or 70%, see Figure 2) during pre-training, and in these settings, the pairwise interactions between patches are under a middle-size context. This implies a possibility that MIM aims to let the model learn to encode interactions of certain complexity, for instance, the interactions of intermediate complexity. To verify this claim, we resort to the tool of multi-order interactions introduced by [12, 56], and investigate whether MIM makes the model more sensitive to interactions of some particular orders. Specifically, the multi-order interaction  $I^{(m)}(i, j)$  is to measure the level of interactions between variables  $i$  and  $j$ . We define  $I^{(m)}(i, j)$  to be the average interaction utility between variables  $i$  and  $j$  on all contexts consisting of  $m$  variables.  $m$  indicates the level of contextual complexity of the interaction. Formally, given an input image  $x$  with a set of  $n$  variables  $N = \{1, \dots, n\}$  (e.g., an image with  $n$  pixels), the multi-order interaction  $I^{(m)}(i, j)$  is defined as:

$$I^{(m)}(i, j) = \mathbb{E}_{S \subseteq N \setminus \{i, j\}, |S|=m} [\Delta f(i, j, S)], \quad (1)$$

where  $\Delta f(i, j, S) = f(S \cup \{i, j\}) - f(S \cup \{i\}) - f(S \cup \{j\}) + f(S)$ .  $f(S)$  indicates the score of output with variables in  $N \setminus S$  kept unchanged but replaced with the baseline value [1], where the context  $S \subseteq N$ . To measure the interaction complexity of the neural network, we measure the relative interaction strength  $J^{(m)}$  of the encoded  $m$ -th order interaction as follows:

$$J^{(m)} = \frac{\mathbb{E}_{x \in \Omega} \mathbb{E}_{i,j} |I^{(m)}(i, j|x)|}{\mathbb{E}_{m'} \mathbb{E}_{x \in \Omega} \mathbb{E}_{i,j} |I^{(m')}(i, j|x)|}, \quad (2)$$

where  $\Omega$  is the set of all samples and  $0 \leq m \leq n - 2$ .  $J^{(m)}$  is the average value over all possible pairs of variables of input samples.  $J^{(m)}$  is normalized by the average value of all interaction strength. The distribution (area under curve sums up to one) of  $J^{(m)}$  indicates the level of interactions of the network. In this work, we use  $J^{(m)}$  as the metric to evaluate and to analyze interaction levels of the network with MIM pre-training. We conduct experiments on IN-100 with image size  $224 \times 224$  and use ViT-S [16] and ResNet-50 [25] as the network architecture. We consider a patch of size  $16 \times 16$  as an input variable. For the computation of  $J^{(m)}$ , we adopt the sampling solution following previous works [12, 56]. As can be seen from Figure 1(e) that ViT-S with random weight initialization tends to learn simple interactions with few patches (e.g., less than  $0.05n$  patches) while MIM pre-trained models show a stronger interaction for relative middle-level (from  $0.05n$  to  $0.5n$ ). Similarly, as observed from 1(g), MIM pre-trained ResNet-50 enhances the middle-level interactions from  $0.1n$  to  $0.55n$  compared to random initialized models. As Figure 1(f) and 1(h) show, MIM pre-training task demonstrates better middle-level interactions compared to contrastive learning pre-training methods for both Transformer and CNN. A stronger middle-level interactions form more complex features such as shape and edge compared to local texture features learned from low-level interactions [33].

### 3.3 From Inpainting to MIM on CNN

It is worth noticing that early inpainting work based on CNN [36] resembles MIM. However, the inpainting task as pre-training on CNNs attracts little attention due to the much inferior performance than contrastive learning methods. We study the resemblance and difference of MIM and Inpainting on CNNs from the feature map perspective. We first plot the log magnitude of Fourier transformed feature maps of ResNet-50 with different pre-training methods on IN-1K [35]. As shown in Figure 3(a), inpainting and MIM show similar low-pass filtering effect at convolution layers as compared to contrastive learning. This indicates that inpainting and MIM reduce noise and uncertainty induced by high-frequency features. However, inpainting as pre-training adopts the masking strategy as illustrated in 1(e) and focuses on the reconstruction performance instead of the patch interactions. We argue that the reconstruction performance of MIM is mainly the patch interaction results of the low or high level while middle-level interactions lead to informative features [12]. Also, the reconstruction performance is not directly related to the learned representation quality. Figure 3(b) shows the feature variance of each layer of ResNet-50 with different pre-training methods on IN-1K. This figure indicates that MIM tends to reduce the feature map variance, and conversely, supervised training, inpainting, and contrastive learning on CNN tend to increase variance. Compared to MIM, which learns better middle-level interactions, inpainting task fails to filter out low-level interactions and thus leads to higher variance. To conclude, MIM enhances middle-level interactions and reduces the feature map uncertainty for a generalized and stabilized feature extraction [34].

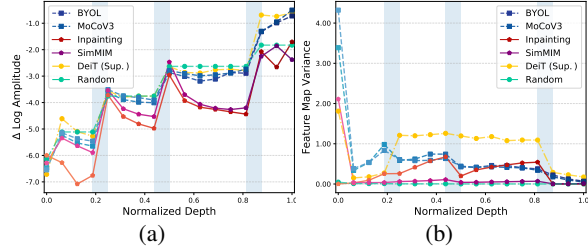


Figure 3: (a) Fourier transformed feature maps. The vertical axis is the relative log amplitudes and the horizontal axis is the normalized depth of the network. The blue columns indicate the pooling layers while the white columns indicate convolution layers. (b) Feature maps variance. The vertical axis is the average variance value of feature maps. DeiT (Sup.) is supervised pre-training.

## 4 Approach

Considering our insight that the essence of MIM is to learn better middle-level interactions for generalized feature extraction, we propose a generic MIM framework following two design rules: (a) **The masking should happen where middle-level interactions occur;** (b) **Guiding the model to**



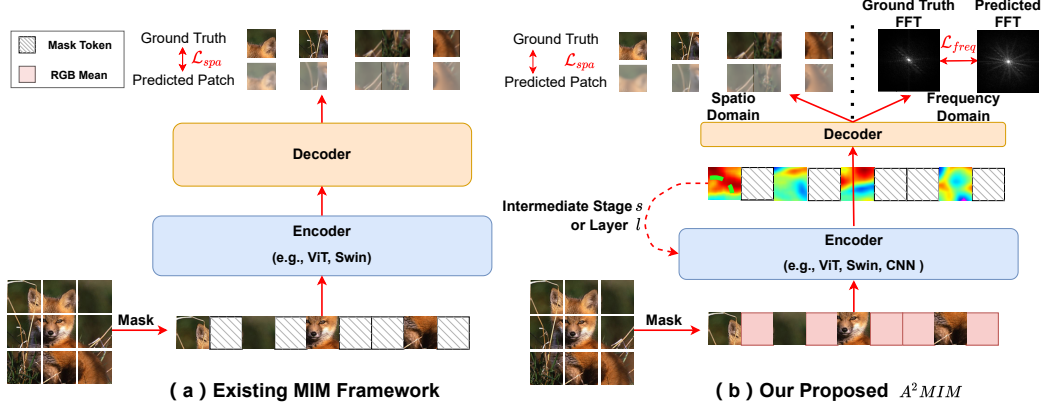


Figure 4: An illustration comparison between existing MIM framework and our proposed framework. For existing MIM framework, the input image is patched into a sequence of patches without overlapping with masked patches replaced with learnable mask tokens. The sequence is then input to the Transformer encoder. The  $\mathcal{L}_{spa}$  is applied between the ground truth patches and the reconstructed patches from the decoder in the spatiotemporal domain. Our proposed framework uses the mean RGB value of the image instead of the mask token in the input space. We then add a learnable mask token onto the intermediate feature map of layer- $l$  of stage- $s$  of the encoder instead of replacement in the input space. The encoder could either be of the Transformer or the CNN family. In addition to the  $\mathcal{L}_{spa}$ , we adopt a  $\mathcal{L}_{freq}$  in the Fourier domain to enhance the encoder to learn more middle-level interactions. Specifically, we apply DFT on both the ground truth image and the predicted image and then use Mean square error (MSE) to measure the difference.

**learn initially neglected target during training.** An overall illustration of our proposed framework in comparison to existing MIM framework is given in Figure 4.

**Mask Token.** For the masking strategy, we follow the common practice of existing works [17, 22, 52, 45] where the input image is divided into non-overlapping patches, and a random subset of patches are masked. MAE utilizes a Transformer as decoder and takes only the visible patches into the encoder. Masked tokens are appended to the decoder to reconstruct the masked patches. simMIM [52] and MaskFeat [45] utilize a fully connected layer as the decoder and feed the mask token into the encoder together with the visible patches. The mask token [13] is a token-shared learnable parameter that indicates the presence of a missing patches to be predicted. Despite different choices of decoder structures, the mask token is either placed at the input to the encoder or the decoder. Mathematically, the masking process of MIM is defined as  $x_{mask} = x \odot (1 - M) + x \odot M$ , where  $M$  is the random occlusion mask and  $T$  represents the learnable mask token. We argue that by masking the image patches as done by current works, the network is picking up low-level interactions. As discussed earlier, we wish to enhance the mid-range interaction of the network and we thus propose to mask intermediate features of the network where information are fused to certain a degree. More concretely, our masking operation is defined as  $z_{mask}^l = z^l + T \odot D(M)$ , where  $z^l$  is the intermediate feature map of  $x$  at layer- $l$  in the Transformer encoder (or denote as  $z^l$  for stage- $s$  in CNNs) and  $D(\cdot)$  is the corresponding down-sampling function of the occlusion mask. We use the average RGB value to fill the masked patches as the input to the encoder. It worth nothing that existing works directly replace the occluded patches with the mask token in the input space or after the patch embedding [16, 4, 52]. In contrast, we replace the occluded patches with the mean of RGB channels of the image and add the mask token onto the intermediate feature maps of the encoder.

**Prediction Target.** Currently proposed works [17, 22, 52] adopt raw RGB values as the prediction target. However, raw pixels are heavy redundant and often contains low-level statistics [4, 45, 60]. Following MAE, Maskfeat [45] proposed to use the Histogram of Oriented Gradients (HOG) as the prediction target outperforming MAE. HOG is a descriptor that captures shape features based on middle-level interactions. Such high-frequency features resulted from middle-level interactions could be well portrayed in the phase component of Fourier spectrum. Given a RGB image  $x \in \mathbb{R}^{3 \times H \times W}$ , the discrete Fourier transform (DFT) of each channel is defined by:

$$F_{(u,v)} = \sum_{h=1}^{h=H} \sum_{w=1}^{w=W} x(h, w) e^{-2\pi j(\frac{uh}{H} + \frac{vw}{W})}. \quad (3)$$

In addition to the common MIM loss in the spatial domain  $\mathcal{L}_{spa}$ , we propose  $\mathcal{L}_{freq}$  to enforce better middle-level interactions in the Fourier domain.  $\mathcal{L}_{freq}$  is defined as:

$$\mathcal{L}_{freq} = \sum_{c=1}^{c=3} \sum_{u=1}^{u=H} \sum_{v=1}^{v=W} \omega(u, v) \odot \|DFT(x_c^{pred} \odot M + \det(x_c^{pred}) \odot (1 - M)) - DFT(x_c)\|, \quad (4)$$

where  $x^{pred}$  is the predicted image,  $\det(\cdot)$  represents the gradient detachment operation and  $\omega(u, v)$  is the frequency weighting matrix as in Focal Frequency Loss[27].  $\omega(u, v)$  is defined as:

$$\omega(u, v) = \|DFT(x_c^{pred} \odot M + \det(x_c^{pred}) \odot (1 - M)) - DFT(x_c)\|^\alpha, \quad (5)$$

where  $\alpha$  is the scaling factor for flexibility ( $\alpha = 1$  in our experiments). It is worth noting that for a 2D signal (one channel of the image), its DFT is conjugate symmetric, which implies that half of the DFT contains the global information. This reduces the prediction target size by half compared to directly predicting missing information from the spatial domain. Moreover, DFT computation is cheap and introduces negligible overhead by using fast Fourier transform (FFT) algorithms (only require  $\mathcal{O}(n \log n)$  complexity) that take advantage of the symmetry and periodicity properties of Fourier transform. The overall loss function of our proposed framework is then defined as:

$$\mathcal{L} = \mathcal{L}_{spa} + \lambda \mathcal{L}_{freq}, \quad (6)$$

where  $\mathcal{L}_{spa} = \|x^{pred} - x\| \odot M$  and  $\lambda$  is a weight parameter to balance the two losses. We set  $\lambda$  to 0.5 by default in this work.

## 5 Experiments

### 5.1 Pre-training Setup.

We adopt ResNet-50 [25] and Vision Transformer [16] (ViT-S/16 and ViT-B/16) as the backbone. We pre-train on ImageNet-1K (IN-1K) training set with AdamW [32] optimizer with the basic learning rate  $1.5e^{-4}$  adjusted by a cosine learning rate scheduler and a batch size of 2048. The input image size is  $224 \times 224$  with a patch size of  $32 \times 32$ . We use a random masking ratio of 60%. By default, the learnable mask tokens are placed at stage-3 in ResNet-50 and layer-5/layer-8 in ViT-S/ViT-B, respectively. We adopt a linear prediction head as the decoder. Our experiments are implemented by Pytorch and conducted on a workstation with NVIDIA V100 GPUs. We report the average results of 3 trials for all experiments, and use **bold** and underline to indicate the best and the second-best performance. See Appendix A for detailed pre-training settings.

### 5.2 Image Classification on ImageNet-1K

**Evaluation Protocols.** We first evaluate the learned representation by end-to-end fine-tuning (FT) and linear probing (Lin.) protocols on IN-1K. For evaluation on CNN, we adopt RSB A2/A3 [46] training settings for fine-tuning on ResNet-50, which employs LAMB [53] optimizer with a cosine

Table 1: ImageNet-1K linear probing (Lin.) and fine-tuning (FT) top-1 accuracy (%) of ResNet-50. Table 2: ImageNet-1K fine-tuning (FT) top-1 accuracy (%) of ViT-S and ViT-B models.

Method	Fast Pre-training			Longer Pre-training			Method	ViT-S		ViT-B	
	Epochs	Lin.	FT (A3)	Epochs	FT (A3)	FT (A2)		Epochs	FT	Epochs	FT
PyTorch (Sup.)	90	76.6	78.8	300	78.9	79.8	DeiT (Sup.)	300	79.9	300	81.8
Inpainting	70	40.1	78.4	-	-	-	DINO	300	80.7	300	82.8
Relative-Loc	70	38.8	77.8	-	-	-	MoCoV3	300	81.4	300	83.2
Rotation	70	48.1	77.7	-	-	-	BEiT	-	-	800	83.2
SimCLR	100	64.4	78.5	800	78.8	79.9	iBOT	800	<b>82.3</b>	400	84.0
MoCoV2	100	66.8	78.5	800	78.8	79.8	PeCo	-	-	800	<b>84.5</b>
BYOL	100	68.4	78.7	400	<u>78.9</u>	80.0	MAE	-	-	1600	83.6
SwAV <sup>†</sup>	100	71.9	<b>78.9</b>	400	<b>79.0</b>	80.2	MaskFeat	-	-	800	84.0
Barlow Twins	100	67.2	78.5	300	78.8	79.9	SimMIM	300	81.7	800	83.8
MoCoV3	100	68.9	78.7	300	<b>79.0</b>	80.1	CAE	300	81.8	800	83.6
SimMIM <sup>‡</sup>	100	47.5	78.2	300	78.1	79.7	CIM	300	81.6	300	83.3
CIM	-	-	-	300	78.6	<u>80.4</u>	<b>A<sup>2</sup>MIM</b>	300	<u>82.2</u>	800	<u>84.2</u>
<b>A<sup>2</sup>MIM</b>	100	48.1	<u>78.8</u>	300	<b>79.0</b>	<b>80.5</b>					

scheduler for 300/100 epochs. For the linear probing setting on ResNet-50, we freeze the backbone features and train a linear classifier with an initial learning rate of 30 and batch size of 256 following MoCo [23]. For evaluation on Transformer, we employ the fine-tuning as MAE [22], which uses DeiT [40] augmentation setting, an AdamW optimizer for 100-epoch training, and adopt a layer-wise learning rate decay of 0.65 following [4]. See Appendix A for detailed evaluation configurations.

**ResNet-50.** We compare the proposed A<sup>2</sup>MIM with classical self-supervised learning methods (Inpainting [36], Relative-Loc [14], and Rotation [19]), contrastive learning, and MIM methods with various pre-training epochs. As shown in Table 1, our approach achieves competitive performance with state-of-the-art contrastive-based methods under 100-epoch RSB A3 fine-tuning. Note that MIM methods see fewer training samples per epoch than contrastive learning methods (40% vs. 200% of patches) and usually require longer pre-training epochs. Based on a longer fine-tuning evaluation using RSB A2, our method (300-epoch) outperforms contrastive-based methods with even fewer training epochs. Meanwhile, our approach also improves the baseline SimMIM<sup>†</sup> [52] (+0.8%) and CIM [18] (+0.4%) in terms of RSB A3 fine-tuning for the longer pre-training. Besides, we also report the linear probing accuracy in the fast pre-training for reference, although our main focus is to learn representations with better fine-tuning performances. The linear probing performance of our method is lower than contrastive-based methods, it still improves the baseline by 0.6%.

**ViT.** We then compare A<sup>2</sup>MIM with recent proposed contrastive-based methods and MIM methods based on ViT-S and ViT-B in Table 2. Our approach outperforms current state-of-the-art methods, *e.g.*, iBOT [60] (MIM with contrastive learning combined) and MaskFeat [45], and improves the baseline SimMIM by 0.5% and 0.4% based on ViT-S and ViT-B. Although the performances of our method are slightly lower than PeCo [15] (online tokenizer required) based on ViT-B, our method is adaptive to both CNN and Transformer architectures.

Table 3: Performance of object detection and seg-Table 4: Performance of object detection and segmentation tasks based on ResNet-50 on COCO and ViT-B on COCO and ADE20K.

Method	Epochs	COCO		ADE-20K mIoU
		AP <sup>box</sup>	AP <sup>mask</sup>	
PyTorch (Sup.)	120	38.2	33.3	36.1
SimCLR	800	37.9	33.3	37.6
MoCoV2	400	39.2	34.3	37.5
BYOL	400	38.9	34.2	37.2
SwAV	800	38.4	33.8	37.3
SimSiam	400	39.2	34.4	37.2
Balow Twins	800	39.2	34.3	37.3
CIM	300	-	-	38.0
<b>A<sup>2</sup>MIM</b>	300	<b>39.8</b>	<b>34.9</b>	<b>38.3</b>

Method	Epochs	COCO		ADE-20K mIoU
		AP <sup>box</sup>	AP <sup>mask</sup>	
DeiT (Sup.)	300	47.9	42.9	47.0
MoCoV3	300	47.9	42.7	47.3
DINO	400	46.8	41.5	47.2
BEiT	300	43.1	38.2	47.1
PeCo	300	43.9	39.8	46.7
MAE	1600	48.5	42.7	48.1
SimMIM	800	48.9	43.0	48.4
CAE	800	49.2	43.3	48.8
<b>A<sup>2</sup>MIM</b>	800	<b>49.3</b>	<b>43.5</b>	<b>49.0</b>

### 5.3 Transfer Learning Experiments

**Object detection and segmentation on COCO.** To verify transferring abilities of self-supervised methods, we benchmark contrastive learning and MIM methods on object detection and segmentation with COCO [31]. For evaluation on CNN, we follow the setup in MoCo [23], which fine-tunes Mask R-CNN [24] with ResNet-50-C4 backbone using  $2\times$  schedule on the COCO *train2017* and evaluates on the COCO *val2017*. Results in Table 3 indicate that our approach (300-epoch) significantly outperforms contrastive-based methods with longer pre-training (+0.7% AP<sup>box</sup> and +0.6% AP<sup>mask</sup>). For evaluation on Transformer, we follow MAE [22], which efficiently fine-tunes Mask R-CNN with ViT-B backbone using  $1\times$  schedule. In Table 4, our approach (800-epoch) is superior to popular contrastive-based and MIM methods, *e.g.*, improves MAE (1600-epoch) by 0.8% AP<sup>box</sup> and 0.8% AP<sup>mask</sup>. The significant performance gain in downstream tasks might be related to capturing more global information during pre-training (see Figure 5).

**Semantic segmentation on ADE20K.** We experiment on ADE-20K [59] using UperNet [49] following MAE [22] to fine-tune the model for 100-epoch with the batch size of 16. Based on ResNet-50, results in Table 3 shows that our method outperforms contrastive learning methods by at least 0.9% mIoU and improves CIM (required extra pre-trained BEiT [4]) by 0.3% mIoU. Based on ViT-B, Table 2 shows that our approach consistently improves MIM methods (*e.g.*, improves MAE and SimMIM by 0.9% and 0.6% mIoU). These observations are consistent with those in COCO.



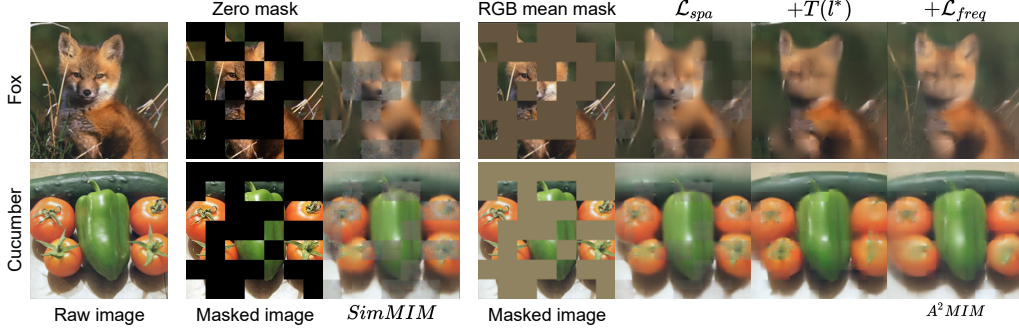


Figure 5: Visualizations of predicted results from SimMIM (middle) and our A<sup>2</sup>MIM (right) based on ViT-S pre-trained 300-epochs on IN-1K. Notice that  $T(l^*)$  denotes the mask token  $T$  to the optimal layer-5 in ViT-S. We ablate the proposed components by adding them to the baseline. Compared to results from SimMIM, reconstruction results ( $\mathcal{L}_{spa}$ ) with the RGB mean mask relieves grid-like artifacts; adding the mask token  $T(l^*)$  further improves the smoothness; using the proposed  $\mathcal{L}_{freq}$  helps the model to capture more informative details and contours.

## 5.4 Ablation Study

To investigate the effectiveness of the proposed components, we conduct ablation studies on ResNet-50 and ViT-S on IN-100 using the fine-tuning protocol. Based on the modified baseline SimMIM, we first compare different mask token mechanisms: **Replacing** denotes the original way in most MIM methods and **Addition** denotes our proposed way that adds the mask token to intermediate feature maps of the backbone. As shown in Figure 6, adding the mask token to the medium stages (stage-3) or layers (layer-5) yields the best performance. Notice that replacing masked patches in input images by RGB channel mean slightly improves the baseline SimMIM, especially for ResNet-50 (88.14 vs. 87.75). Then, we verify the proposed  $\mathcal{L}_{freq}$  in Table 5. We find that simply using  $\mathcal{L}_{freq}$  without the adaptive re-weighting  $\omega$  (Eqn. 5) brings some improvements as the frequency constraint to  $\mathcal{L}_{spa}$ , while employing  $\omega$  further enhances the performance by helping the model to learn more informative frequency components. Additionally, we visualize reconstruction results in Figure 5 to domesticate the improvements brought by our proposed components (see more visualization results in Appendix B).

Figure 6: Ablation of mask token in various stages (S) or layers (L) based on SimMIM (without  $\mathcal{L}_{freq}$ ) on IN-100.

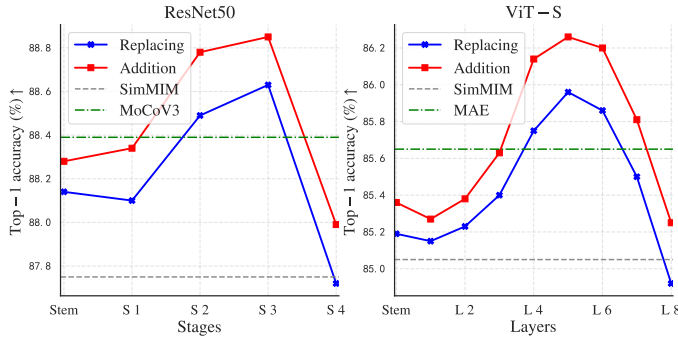


Table 5: Ablation of proposed  $\mathcal{L}_{freq}$  on IN-100. w/o  $\omega$  denotes removing the re-weighting term  $\omega$  in  $\mathcal{L}_{freq}$  and  $T(l^*)$  denotes adding the mask token  $T$  to the optimal layer- $l^*$ .

	ResNet-50	ViT-S
$\mathcal{L}_{spa}$	88.19	85.17
$+\mathcal{L}_{freq}$ w/o $\omega$	88.47	86.05
$+\mathcal{L}_{freq}$	88.73	86.41
$+\mathcal{L}_{freq} + T(l^*)$	<b>88.86</b>	<b>86.62</b>

## 6 Conclusion

In this paper, we delved deep into MIM and answer the question of what exactly is learned during MIM pre-training. We adopted the multi-order interactions to study the interaction level among image patches. We discovered that MIM is essentially teaching the network to learn middle-level interactions among image patches for more complex feature extraction regardless of the network architecture. Based on our findings, we further proposed a general framework A<sup>2</sup>MIM that is compatible with both Transformers and CNNs for MIM tasks aiming at enhancing patch interactions during self-supervised pre-training. Besides a different mask token mechanism, we proposed a loss in the Fourier domain to better learn the middle-level interaction. Experimental results have shown that our proposed framework improves the representations learned for both CNNs and Transformers yielding superior performance than state-of-the-arts on various downstream tasks.

## References

- [1] Marco Ancona, Cengiz Oztireli, and Markus Gross. Explaining deep neural networks with a polynomial time algorithm for shapley value approximation. In *International Conference on Machine Learning*, pages 272–281. PMLR, 2019.
- [2] Mahmoud Assran, Mathilde Caron, Ishan Misra, Piotr Bojanowski, Florian Bordes, Pascal Vincent, Armand Joulin, Michael Rabbat, and Nicolas Ballas. Masked siamese networks for label-efficient learning. *arXiv preprint arXiv:2204.07141*, 2022.
- [3] Alexei Baevski, Wei-Ning Hsu, Qiantong Xu, Arun Babu, Jiatao Gu, and Michael Auli. Data2vec: A general framework for self-supervised learning in speech, vision and language. *arXiv preprint arXiv:2202.03555*, 2022.
- [4] Hangbo Bao, Li Dong, and Furu Wei. Beit: Bert pre-training of image transformers. *arXiv preprint arXiv:2106.08254*, 2021.
- [5] Mathilde Caron, Ishan Misra, Julien Mairal, Priya Goyal, Piotr Bojanowski, and Armand Joulin. Unsupervised learning of visual features by contrasting cluster assignments. *Advances in Neural Information Processing Systems*, 33:9912–9924, 2020.
- [6] Mathilde Caron, Hugo Touvron, Ishan Misra, Hervé Jégou, Julien Mairal, Piotr Bojanowski, and Armand Joulin. Emerging properties in self-supervised vision transformers. In *Proceedings of the International Conference on Computer Vision (ICCV)*, 2021.
- [7] Mark Chen, Alec Radford, Rewon Child, Jeffrey Wu, Heewoo Jun, David Luan, and Ilya Sutskever. Generative pretraining from pixels. In *International Conference on Machine Learning*, pages 1691–1703. PMLR, 2020.
- [8] Ting Chen, Simon Kornblith, Mohammad Norouzi, and Geoffrey Hinton. A simple framework for contrastive learning of visual representations. *arXiv preprint arXiv:2002.05709*, 2020.
- [9] Xinlei Chen and Kaiming He. Exploring simple siamese representation learning. *arXiv preprint arXiv:2011.10566*, 2020.
- [10] Xinlei Chen, Saining Xie, and Kaiming He. An empirical study of training self-supervised vision transformers. In *Proceedings of the IEEE/CVF International Conference on Computer Vision*, pages 9640–9649, 2021.
- [11] Ekin D Cubuk, Barret Zoph, Jonathon Shlens, and Quoc V Le. Randaugment: Practical automated data augmentation with a reduced search space. In *Proceedings of the IEEE/CVF Conference on Computer Vision and Pattern Recognition Workshops*, pages 702–703, 2020.
- [12] Huiqi Deng, Qihan Ren, Xu Chen, Hao Zhang, Jie Ren, and Quanshi Zhang. Discovering and explaining the representation bottleneck of dnns. In *International Conference on Learning Representations (ICLR)*, 2022.
- [13] Jacob Devlin, Ming-Wei Chang, Kenton Lee, and Kristina Toutanova. Bert: Pre-training of deep bidirectional transformers for language understanding. *arXiv preprint arXiv:1810.04805*, 2018.
- [14] Carl Doersch, Abhinav Gupta, and Alexei A Efros. Unsupervised visual representation learning by context prediction. In *Proceedings of the International Conference on Computer Vision (ICCV)*, 2015.
- [15] Xiaoyi Dong, Jianmin Bao, Ting Zhang, Dongdong Chen, Weiming Zhang, Lu Yuan, Dong Chen, Fang Wen, and Nenghai Yu. Peco: Perceptual codebook for bert pre-training of vision transformers. *arXiv preprint arXiv:2111.12710*, 2021.
- [16] Alexey Dosovitskiy, Lucas Beyer, Alexander Kolesnikov, Dirk Weissenborn, Xiaohua Zhai, Thomas Unterthiner, Mostafa Dehghani, Matthias Minderer, Georg Heigold, Sylvain Gelly, et al. An image is worth 16x16 words: Transformers for image recognition at scale. *arXiv preprint arXiv:2010.11929*, 2020.
- [17] Alaaeldin El-Nouby, Gautier Izacard, Hugo Touvron, Ivan Laptev, Hervé Jégou, and Edouard Grave. Are large-scale datasets necessary for self-supervised pre-training? *arXiv preprint arXiv:2112.10740*, 2021.
- [18] Yuxin Fang, Li Dong, Hangbo Bao, Xinggang Wang, and Furu Wei. Corrupted image modeling for self-supervised visual pre-training. *arXiv preprint arXiv:2202.03382*, 2022.
- [19] Spyros Gidaris, Praveer Singh, and Nikos Komodakis. Unsupervised representation learning by predicting image rotations. In *International Conference on Learning Representations (ICLR)*, 2018.
- [20] Priya Goyal, Piotr Dollár, Ross Girshick, Pieter Noordhuis, Lukasz Wesolowski, Aapo Kyrola, Andrew Tulloch, Yangqing Jia, and Kaiming He. Accurate, large minibatch sgd: Training imagenet in 1 hour. *arXiv preprint arXiv:1706.02677*, 2020.
- [21] Jean-Bastien Grill, Florian Strub, Florent Altché, Corentin Tallec, Pierre H Richemond, Elena Buchatskaya, Carl Doersch, Bernardo Avila Pires, Zhaohan Daniel Guo, Mohammad Gheshlaghi Azar, et al. Bootstrap your own latent: A new approach to self-supervised learning. In *NeurIPS*, 2020.

- [22] Kaiming He, Xinlei Chen, Saining Xie, Yanghao Li, Piotr Dollár, and Ross Girshick. Masked autoencoders are scalable vision learners. *arXiv preprint arXiv:2111.06377*, 2021.
- [23] Kaiming He, Haoqi Fan, Yuxin Wu, Saining Xie, and Ross Girshick. Momentum contrast for unsupervised visual representation learning. In *Proceedings of the IEEE/CVF Conference on Computer Vision and Pattern Recognition*, pages 9729–9738, 2020.
- [24] Kaiming He, Georgia Gkioxari, Piotr Dollár, and Ross Girshick. Mask r-cnn. In *Proceedings of the International Conference on Computer Vision (ICCV)*, 2017.
- [25] Kaiming He, Xiangyu Zhang, Shaoqing Ren, and Jian Sun. Deep residual learning for image recognition. In *Proceedings of the IEEE conference on computer vision and pattern recognition*, pages 770–778, 2016.
- [26] Geoffrey E Hinton and Richard Zemel. Autoencoders, minimum description length and helmholtz free energy. *Advances in neural information processing systems*, 6, 1993.
- [27] Liming Jiang, Bo Dai, Wayne Wu, and Chen Change Loy. Focal frequency loss for image reconstruction and synthesis. In *Proceedings of the IEEE/CVF International Conference on Computer Vision*, pages 13919–13929, 2021.
- [28] Alex Krizhevsky, Ilya Sutskever, and Geoffrey E Hinton. Imagenet classification with deep convolutional neural networks. In F. Pereira, C. J. C. Burges, L. Bottou, and K. Q. Weinberger, editors, *Advances in Neural Information Processing Systems*, volume 25. Curran Associates, Inc., 2012.
- [29] Alex Krizhevsky, Ilya Sutskever, and Geoffrey E Hinton. Imagenet classification with deep convolutional neural networks. In *Advances in neural information processing systems*, pages 1097–1105, 2012.
- [30] Tsung-Yi Lin, Piotr Dollar, Ross Girshick, Kaiming He, Bharath Hariharan, and Serge Belongie. Feature pyramid networks for object detection. In *Proceedings of the IEEE Conference on Computer Vision and Pattern Recognition (CVPR)*, July 2017.
- [31] Tsung-Yi Lin, Michael Maire, Serge Belongie, James Hays, Pietro Perona, Deva Ramanan, Piotr Dollár, and C Lawrence Zitnick. Microsoft coco: Common objects in context. In *Proceedings of the European Conference on Computer Vision (ECCV)*, 2014.
- [32] Ilya Loshchilov and Frank Hutter. Decoupled weight decay regularization. In *International Conference on Learning Representations (ICLR)*, 2019.
- [33] Muhammad Muzammal Naseer, Kanchana Ranasinghe, Salman H Khan, Munawar Hayat, Fahad Shah-baz Khan, and Ming-Hsuan Yang. Intriguing properties of vision transformers. *Advances in Neural Information Processing Systems*, 34, 2021.
- [34] Namuk Park and Songkuk Kim. Blurs behave like ensembles: Spatial smoothings to improve accuracy, uncertainty, and robustness. *arXiv preprint arXiv:2105.12639*, 2021.
- [35] Namuk Park and Songkuk Kim. How do vision transformers work? In *International Conference on Learning Representations (ICLR)*, 2022.
- [36] Deepak Pathak, Philipp Krahenbuhl, Jeff Donahue, Trevor Darrell, and Alexei A Efros. Context encoders: Feature learning by inpainting. In *Proceedings of the IEEE conference on computer vision and pattern recognition*, pages 2536–2544, 2016.
- [37] Alec Radford, Karthik Narasimhan, Tim Salimans, and Ilya Sutskever. Improving language understanding by generative pre-training (2018), 2018.
- [38] Ramprasaath R Selvaraju, Karan Desai, Justin Johnson, and Nikhil Naik. Casting your model: Learning to localize improves self-supervised representations. In *Proceedings of the IEEE/CVF Conference on Computer Vision and Pattern Recognition (CVPR)*, pages 11058–11067, 2021.
- [39] Yonglong Tian, Dilip Krishnan, and Phillip Isola. Contrastive multiview coding. In *Proceedings of the European Conference on Computer Vision (ECCV)*, 2020.
- [40] Hugo Touvron, Matthieu Cord, Matthijs Douze, Francisco Massa, Alexandre Sablayrolles, and Hervé Jégou. Training data-efficient image transformers & distillation through attention. In *International Conference on Machine Learning*, pages 10347–10357. PMLR, 2021.
- [41] Aaron Van den Oord, Yazhe Li, and Oriol Vinyals. Representation learning with contrastive predictive coding. *arXiv e-prints*, pages arXiv–1807, 2018.
- [42] Ashish Vaswani, Noam Shazeer, Niki Parmar, Jakob Uszkoreit, Llion Jones, Aidan N Gomez, Łukasz Kaiser, and Illia Polosukhin. Attention is all you need. *Advances in neural information processing systems*, 30, 2017.
- [43] Pascal Vincent, Hugo Larochelle, Yoshua Bengio, and Pierre-Antoine Manzagol. Extracting and composing robust features with denoising autoencoders. In *Proceedings of the 25th international conference on Machine learning*, pages 1096–1103, 2008.

- [44] Pascal Vincent, Hugo Larochelle, Isabelle Lajoie, Yoshua Bengio, Pierre-Antoine Manzagol, and Léon Bottou. Stacked denoising autoencoders: Learning useful representations in a deep network with a local denoising criterion. *Journal of machine learning research*, 11(12), 2010.
- [45] Chen Wei, Haoqi Fan, Saining Xie, Chao-Yuan Wu, Alan Yuille, and Christoph Feichtenhofer. Masked feature prediction for self-supervised visual pre-training. *arXiv preprint arXiv:2112.09133*, 2021.
- [46] Ross Wightman, Hugo Touvron, and Hervé Jégou. Resnet strikes back: An improved training procedure in timm, 2021.
- [47] Di Wu, Siyuan Li, Zelin Zang, Kai Wang, Lei Shang, Baigui Sun, Hao Li, and Stan Z Li. Align yourself: Self-supervised pre-training for fine-grained recognition via saliency alignment. *arXiv preprint arXiv:2106.15788*, 2021.
- [48] Zhirong Wu, Yuanjun Xiong, X Yu Stella, and Dahua Lin. Unsupervised feature learning via non-parametric instance discrimination. In *Proceedings of the IEEE Conference on Computer Vision and Pattern Recognition (CVPR)*, 2018.
- [49] Tete Xiao, Yingcheng Liu, Bolei Zhou, Yuning Jiang, and Jian Sun. Unified perceptual parsing for scene understanding. In *European Conference on Computer Vision (ECCV)*. Springer, 2018.
- [50] Tete Xiao, Colorado J Reed, Xiaolong Wang, Kurt Keutzer, and Trevor Darrell. Region similarity representation learning. *arXiv preprint arXiv:2103.12902*, 2021.
- [51] Enze Xie, Jian Ding, Wenhai Wang, Xiaohang Zhan, Hang Xu, Zhenguo Li, and Ping Luo. Detco: Unsupervised contrastive learning for object detection. In *Proceedings of the International Conference on Computer Vision (ICCV)*, 2021.
- [52] Zhenda Xie, Zheng Zhang, Yue Cao, Yutong Lin, Jianmin Bao, Zhuliang Yao, Qi Dai, and Han Hu. Simsim: A simple framework for masked image modeling. *arXiv preprint arXiv:2111.09886*, 2021.
- [53] Yang You, Jing Li, Sashank Reddi, Jonathan Hseu, Sanjiv Kumar, Srinadh Bhojanapalli, Xiaodan Song, James Demmel, Kurt Keutzer, and Cho-Jui Hsieh. Large batch optimization for deep learning: Training BERT in 76 minutes. In *International Conference on Learning Representations (ICLR)*, 2020.
- [54] Sangdoo Yun, Dongyoon Han, Seong Joon Oh, Sanghyuk Chun, Junsuk Choe, and Youngjoon Yoo. Cutmix: Regularization strategy to train strong classifiers with localizable features. In *Proceedings of the IEEE/CVF international conference on computer vision*, pages 6023–6032, 2019.
- [55] Jure Zbontar, Li Jing, Ishan Misra, Yann LeCun, and Stéphane Deny. Barlow twins: Self-supervised learning via redundancy reduction. In *International Conference on Machine Learning*, pages 12310–12320. PMLR, 2021.
- [56] Hao Zhang, Sen Li, Yinchao Ma, Mingjie Li, Yichen Xie, and Quanshi Zhang. Interpreting and boosting dropout from a game-theoretic view. *arXiv preprint arXiv:2009.11729*, 2020.
- [57] Richard Zhang, Phillip Isola, and Alexei A Efros. Colorful image colorization. In *Proceedings of the European Conference on Computer Vision (ECCV)*, 2016.
- [58] Zhun Zhong, Liang Zheng, Guoliang Kang, Shaozi Li, and Yi Yang. Random erasing data augmentation. In *Proceedings of the AAAI conference on artificial intelligence*, volume 34, pages 13001–13008, 2020.
- [59] Bolei Zhou, Hang Zhao, Xavier Puig, Tete Xiao, Sanja Fidler, Adela Barriuso, and Antonio Torralba. Semantic understanding of scenes through the ade20k dataset. *International Journal of Computer Vision (IJCV)*, 2019.
- [60] Jinghao Zhou, Chen Wei, Huiyu Wang, Wei Shen, Cihang Xie, Alan Yuille, and Tao Kong. ibot: Image bert pre-training with online tokenizer. *arXiv preprint arXiv:2111.07832*, 2021.

## A Details of Comparison Experiments

This section provides experimental details for Sec. 5, e.g., pre-training and evaluation on ImageNet-1K and transfer learning settings on downstream tasks.

### A.1 ImageNet-1K Experiments

**Pre-training.** The default settings of A<sup>2</sup>MIM for ResNet-50 and ViTs are provided in Table A1, following SimMIM [52]. We use AdamW [32] optimizer with the cosine scheduler and the linear learning rate scaling rule [20]:  $lr = base\_lr \times \text{batchsize} / 256$ . Similar to current MIM methods, we only use RandomResizedCrop with the scale of (0.67, 1.0) and do not require other complex augmentations (e.g., Rand Augment [11], mixups [54], or stochastic depth) during pre-training.

**End-to-end fine-tuning.** Our fine-tuning follow common practices of supervised image classification on ImageNet-1K. As shown in Table A2, we fine-tune pre-trained ViTs for 100 epochs using the DeiT [40] training recipe, which employs AdamW [32] optimizer with the cross-entropy (CE) loss; we fine-tune pre-trained ResNet-50 for 100/300 epochs using RSB A3/A2 [46] settings, which employs LAMB [53] optimizer with the binary cross-entropy (BCE) loss. Additionally, we use layer-wise learning rate decay as [4] for fine-tuning ViT models.

Table A1: ImageNet-1K A<sup>2</sup>MIM pre-training settings for ResNet-50 and ViT models.

Configuration	ResNet-50	ViTs
Pre-training resolution	224	224
Mask patch size	32	32
Optimizer	AdamW	AdamW
Base learning rate	1.5e-4	1e-4
Weight decay	0.05	0.05
Optimizer momentum	$\beta_1, \beta_2=0.9, 0.999$	$\beta_1, \beta_2=0.9, 0.999$
Batch size	2048	2048
Learning rate schedule	cosine decay	cosine decay
Warmup epochs	10	10
RandomResizedCrop	✓	✓
Rand Augment	✗	✗
Stochastic Depth	✗	✗
Gradient Clipping	✗	5

Table A2: ImageNet-1K fine-tuning recipes for ResNet-50 (RSB A2/A3) and ViTs (DeiT).

Configuration	ViTs	ResNet-50	
	DeiT	RSB A2	RSB A3
FT epochs	100	300	100
Training resolution	224	224	160
Testing resolution	224	224	224
Testing crop ratio	0.875	0.95	0.95
Optimizer	AdamW	LAMB	LAMB
Base learning rate	$2.5 \times 10^{-4}$	$1.5 \times 10^{-3}$	$1 \times 10^{-3}$
Weight decay	0.05	0.02	0.02
Batch size	1024	2048	2048
Learning rate schedule	cosine decay	cosine decay	cosine decay
Warmup epochs	5	5	5
Label smoothing $\epsilon$	0.1	✗	✗
Stochastic depth	0.1	0.05	✗
Gradient clipping	5.0	✗	✗
Rand Augment	(9, 0.5)	(7, 0.5)	(6, 0.5)
Mixup alpha	0.8	0.1	0.1
CutMix alpha	1.0	1.0	1.0
Loss function	CE loss	BCE loss	BCE loss

### A.2 Object Detection and Segmentation on COCO

We adopt Mask-RCNN [24] framework to perform transfer learning to object detection and segmentation on COCO [31] in Detectron2<sup>2</sup>. For evaluation on ResNet-50, we follow MoCo [23] and fine-tune Mask R-CNN with the pre-trained ResNet-50-C4 backbone using  $2\times$  schedule (24 epochs). For evaluation of ViTs, we follow MAE [22], which employs the pre-trained ViT backbone and an FPN neck [30] in Mask R-CNN, and fine-tune the model using  $1\times$  schedule (12 epochs). For a fair comparison, we follow [4, 52] to turn on relative position bias in ViT [16] during both pre-training and transfer learning, initialized as zero.

### A.3 Semantic Segmentation on ADE-20K

We adopt UperNet [49] to perform transfer learning to semantic segmentation on ADE-20K and use the semantic segmentation implementation in MMSegmentation<sup>3</sup>. We initialize the UperNet using the pre-trained backbones (ResNet-50 or ViTs) on ImageNet-1K and fine-tune end-to-end for 100 epochs with a batch size of 16. We search for the optimal  $lr$  for all competitors. Similar to fine-tuning settings on COCO, we use relative position bias in ViT [16] during both pre-training and transfer learning as [4, 52].

<sup>2</sup><https://github.com/facebookresearch/detectron2>

<sup>3</sup><https://github.com/open-mmlab/mms Segmentation>



## B Empirical Experiments

### B.1 Occlusion Robustness

In Sec. 3.1, we analyze robustness against occlusion of fine-tuned models on ImageNet-100 (a subset on ImageNet-1K divided by [39]) using the official implementation<sup>4</sup> provided by [33]. Both MIM and contrastive-based methods are pre-trained 400 epochs on ImageNet-100 using their pre-training settings on ImageNet-1K. We adopt the fine-tuning training recipe as DeiT in Table A2 and use the same setting (100-epoch) for both ViT-S and ResNet-50. Note that we use the modified SimMIM for ResNet-50 (replacing masked patches in the input image with the RGB mean) in all experiments. As shown in Figure 1, we compared MIM pre-trained models supervised methods with various augmentations and contrastive learning pre-trained methods in terms of the top-1 accuracy under various occlusion ratios. Note that the occlusion ratio means the ratio of dropped and total patches and we plot the mean of accuracy across 3 runs. We can conclude that MIM pre-trained models have stronger robustness against occlusion compared to supervised and contrastive-based methods.

### B.2 Multi-order Interaction

In Sec. 3.2, we interpret what is learned by MIM by multi-order interaction [12, 56]. The interaction complexity can be represented by  $I^{(m)}(i, j)$  (defined in Eqn. 1), which measures the average interaction utility between variables  $i, j$  on all contexts consisting of  $m$  variables. Notice that the order  $m$  reflects the contextual complexity of the interaction  $I^{(m)}(i, j)$ . For example, a low-order interaction (e.g.,  $m = 0.05n$ ) means the relatively simple collaboration between variables  $i, j$ , while a high-order interaction (e.g.,  $m = 0.05n$ ) corresponds to the complex collaboration. As figured out in the representation bottleneck [12], deep neural networks (DNNs) are more likely to encode both low-order interactions and high-order interactions, but often fail to learn middle-order interactions. We hypothesize that MIM helps models learn more middle-level interactions since MIM has a natural advantage in cases where some parts of the image are masked out. In Figure 1, we calculate the interaction strength  $J^{(m)}$  (defined in Eqn. 2) for fine-tuned models on ImageNet-100 using the official implementation<sup>5</sup> provided by [12]. Specially, we use the image of  $224 \times 224$  resolution as the input and calculate  $J^{(m)}$  on  $14 \times 14$  grids, i.e.,  $n = 14 \times 14$ . And we set the model output as  $f(x_S) = \log \frac{P(\hat{y}=y|x_S)}{1-P(\hat{y}=y|x_S)}$  given the masked sample  $x_S$ , where  $y$  denotes the groundtruth label and  $P(\hat{y} = y|x_S)$  denotes the probability of classifying the masked sample  $x_S$  to the true category. In addition to Sec. 3.2, we further provide occlusion robustness results and interaction strength for ResNet-50 on ImageNet-1K in Figure A1. These observations are consistent with those in Sec. 3.

### B.3 Analysis of Feature Maps

In Sec. 3.3, we perform Fourier and variant analysis of feature maps in pre-trained ResNet-50 on ImageNet-1K. Following [35], we first convert feature maps into the frequency domain and represent them on the normalized frequency domain (the highest frequency components are at  $\{-\pi, +\pi\}$ ). In Figure 3(a), we report the amplitude ratio of high-frequency components by using  $\Delta \log$  amplitude, and find that inpainting and MIM reduce high-frequency components at convolution layers compared to supervised and contrastive learning. Then, we provide the standard deviation of feature maps by block depth as [35, 34] in Figure 3(b), which shows that MIM tends to reduce feature map variances compared to other pre-training methods. Notice that we also plot results of the randomly initialized network in Figure 3 for reference. Therefore, we conclude that MIM learns features with less uncertainty than supervised and contrastive learning methods.

## C Visualization Experimental Details

In addition to Sec. 5.4, we provide more visualization results of A<sup>2</sup>MIM. Similar to Figure 5, we ablate the proposed components in A<sup>2</sup>MIM based on ResNet-50 in Figure A2, which demonstrates that A<sup>2</sup>MIM helps ResNet-50 learn more spatial details, i.e., more middle-level interactions. Moreover, we study the effects of the mask token in both ViTs and CNNs in Figure A3.

<sup>4</sup><https://github.com/Muzammal-Naseer/Intriguing-Properties-of-Vision-Transformers>

<sup>5</sup><https://github.com/Nebularaid2000/bottleneck>

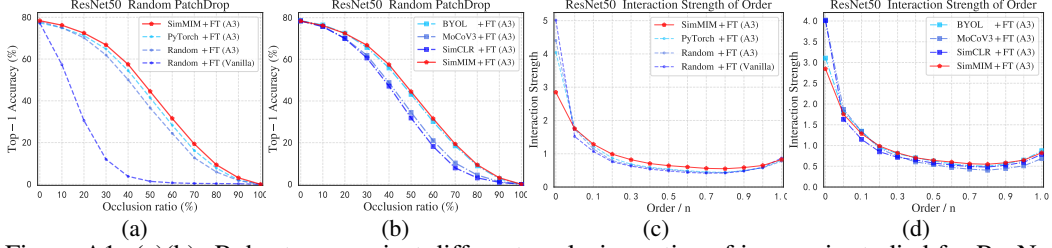


Figure A1: (a)(b): Robustness against different occlusion ratios of images is studied for ResNet-50 under various experimental settings on ImageNet-1K. (c)(d): Distributions of the interaction strength  $J^{(m)}$  is explored for ResNet-50 under various experimental settings. The label indicates the pre-training method + fine-tuning setting used, random stands for random weight initialization.

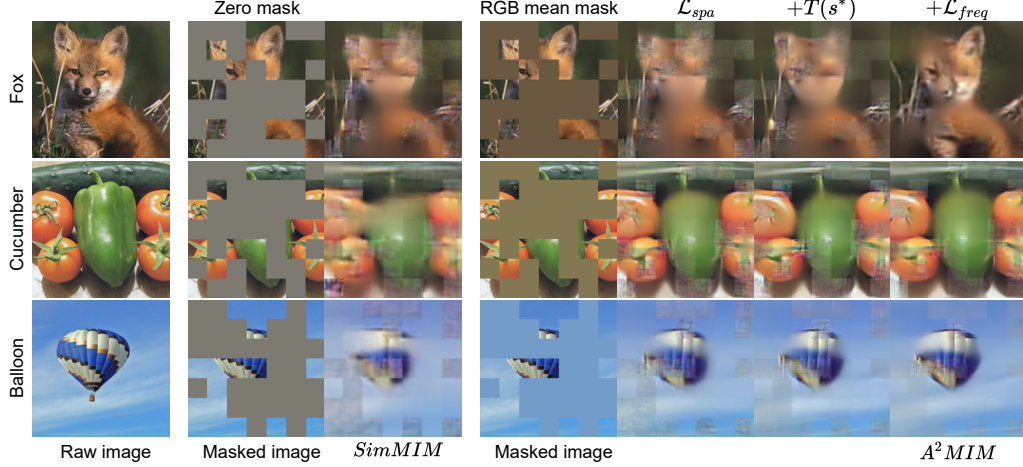


Figure A2: Visualizations of predicted results from SimMIM (middle) and our  $A^2MIM$  (right) based on ResNet-50 pre-trained 100-epochs on ImageNet-1K. Notice that  $T(s^*)$  denotes the mask token  $T$  to the optimal stage- $s$  in ResNet-50. We ablate the proposed components by adding them to the baseline SimMIM: replacing the zero mask with the RGB mean mask and adding the mask token  $T(s^*)$  relieve grid-like artifacts in predicted results; adding the proposed  $\mathcal{L}_{freq}$  helps the model to capture more informative details.

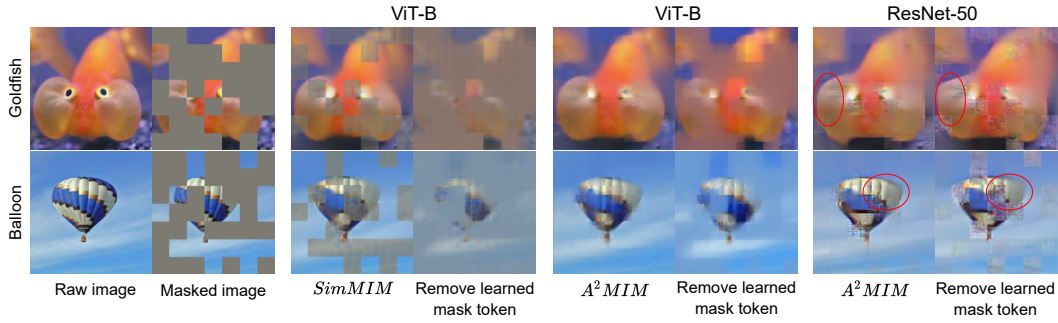


Figure A3: Visualizations of predicted results with and without the mask token on ImageNet-1K. Notice that mask tokens are adopted in the pre-trained models based on ViT-S (300-epoch) or ResNet-50 (100-epoch). Based on ViT-S, removing the mask token corrupts both contents of masked patches and overall colors in SimMIM while only corrupting the masked contents in  $A^2MIM$ . Based on ResNet-50, removing the mask token slightly affects spatial details in the masked patches and causes grid-like artifacts in the unmasked patches. The different effects of the mask token in ViT-S and ResNet-50 might be because the two architectures use different spatial-mixing operators and normalization layers. As for ViTs, the self-attention operation captures informative details from unmasked patches, but the non-overlap patch embedding and layer normalization mask each patch isolated. The mask token learns the mean templates (contents) of masked patches and gathers spatial details from unmasked patches by the self-attention operation. As for CNNs, each patch shares the same contents from the batch normalization, and the convolution operation extract features from unmasked and masked patches equally. The mask token learns more high-frequency and informative details.